Radiative neutron capture cross section from ^{236}U

B. Baramsai, M. Jandel, T. A. Bredeweg, E. M. Bond, A. R. Roman, G. Rusev, C. L. Walker, A. Couture, S. Mosby, J. M. O'Donnell, J. L. Ullmann, and T. Kawano

Phys. Rev. C **96**, 024619 — Published 24 August 2017

DOI: 10.1103/PhysRevC.96.024619

Radiative neutron capture cross section from ^{236}U

B. Baramsai,* M. Jandel, T. A. Bredeweg, E. M. Bond, A. R. Roman, G. Rusev, and C. L. Walker
Chemistry Division, Los Alamos National Laboratory, Los Alamos, New Mexico 87545, USA

A. Couture, S. Mosby, J. M. O'Donnell, and J. L. Ullmann
Physics Division, Los Alamos National Laboratory, Los Alamos, New Mexico 87545, USA

T. Kawano
Theory Division, Los Alamos National Laboratory, Los Alamos, New Mexico 87545, USA
(Dated: April 10, 2017)

The ^{236}U(n,γ) reaction cross section has been measured for the incident neutron energy range from 10 eV to 800 keV using the DANCE γ-ray calorimeter at the Los Alamos Neutron Science Center. The cross section was determined with the ratio method, a novel technique using the ^{235}U(n,f) reaction as a reference. The results of the experiment are reported in the resolved and unresolved resonance energy regions. Individual neutron resonance parameters were obtained below 1 keV incident energy using the R-Matrix code SAMMY. The cross section in the unresolved resonance region is determined with improved experimental uncertainty. It agrees with both ENDF/B-VII.1 and JEFF-3.2 nuclear data libraries. The results above 10 keV agree better with the JEFF-3.2 library.

PACS numbers: 25.40.Ny, 24.30.-v, 21.10.Hw, 21.10.Ma

I. INTRODUCTION

Neutron capture reaction data are important for many applications including stockpile stewardship, advanced fuel cycle reactors, nuclear astrophysics and fundamental nuclear physics. The capture cross section of ^{236}U is particularly important in addressing the build-up of higher actinides in nuclear fuel, the burn up of actinides, the activation of spent fuel and reprocessing radioactive waste. The current ^{236}U(n,γ) cross section data are not sufficient for the design of future reactors such as Fast Reactors and Thorium fuel cycle based, accelerator-driven systems [1]. The uncertainty assessment of the evaluated nuclear data of major and minor actinides recommends improving the uncertainty of the ^{236}U capture cross section by carrying out new measurements [2].

Earlier experimental data were mostly based on activation measurements. The first activation measurement with reactor neutrons was carried out by P. Hubbert *et al.* [3] at CEA/Saclay, France in 1955 and a similar measurement by B. V. Efimov *et al.* [4], in 1956. The thermal cross sections of the two measurements were consistent. Later, activation measurements in the fast neutron region were made by J. F. Barry *et al.* [5] using the Van de Graaf accelerator, and the same measurement was also reported by D. C. Stupegia *et al.* [6] from Argonne National Laboratory. Both measurements overestimate the neutron capture cross section as shown in Fig. 1.

The first neutron absorption experiment in the resolved resonance region was performed by Harvey and Hughes [7] in 1958, and the latest experiment was performed by Macklin *et al.* [8] in 1990. A capture cross section and resonance analysis was performed by Carlson *et al.* [9] with both neutron capture and absorption data using several highly enriched ^{236}U targets with different thicknesses.

Direct measurements of the neutron capture cross section are relatively sparse. As it is shown in Fig. 1, cross section data from earlier measurements have large discrepancies. The most recent measurements on the ^{236}U(n,γ) reaction were performed at the GELINA facility in Geel, Belgium [10], the nTOF facility in CERN [11] and by Muradyan *et al.* at the Kurchatov Institute in Moscow [12]. The nTOF measurement was performed with a pair of C_6D_6 detectors and the 4π BaF_2 Total Absorption Calorimeter. The nTOF preliminary data [11] in the unresolved resonance region is in agreement with current evaluations with a systematic uncertainty of 7%. They reported some discrepancies in the resonance region. The resonance energies were found to be systematically lower compared to current evaluation. Average cross section data of the other two measurements [10, 12] are in agreement with evaluated cross section data within the statistical uncertainties.

We have performed a series of experiments on the ^{236}U(n,γ) reaction using the Detector for Advanced Neutron Capture Experiments (DANCE) located at the Los Alamos Neutron Science Center (LANSCE). DANCE has the capability to measure capture γ-rays with good timing resolution and a high γ-ray detection efficiency that makes it a unique facility for the high precision (n,γ) cross section measurements [13]. The experiments were mainly carried out in two separate beam cycles because of beam time availability. We also used earlier experimental data from ^{235}U(n,f) taken in the 2011 beam cycles to benchmark the applicability of the ratio method outlined in [14]. The latest data were collected in 2015 when the

* bayar@lanl.gov

DANCE Data Acquisition System (DAQ) was upgraded with 14 bit, 500 MHz, V1730B CAEN digitizers [15]. The DAQ upgrade gives us an advantage to continue the measurement over the entire 50 ms of a beam spill rather than the 500 μs limit of the old DAQ. The analysis of the latest measurement yields cross section values from the thermal to 1 MeV incident neutron energy region.

We report the results for the (n,γ) cross section in two different energy regions, the resonance region from 10 eV to 1 keV and the unresolved resonance region from 1 keV to 800 keV. The fission cross section on ^{236}U is negligible compared to the capture cross section up to 800 keV. A detailed analysis of the resonance region of the cross section gives complementary information about the average quantities of the compound nuclear

reaction such as s-wave level spacing, neutron and radiation widths.

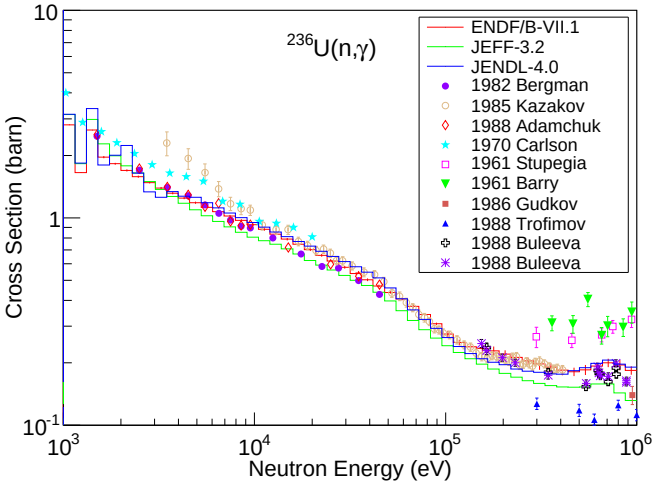

FIG. 1. Earlier ^{236}U(n,γ) cross-section measurements [9–12] compared to the evaluated nuclear data ENDF/B-VII.1 [16] and JEFF-3.2 [17]

II. EXPERIMENT

The neutron beam at LANSCE is produced by the spallation reaction of 800 MeV accelerated protons irradiating a tungsten target and is moderated in a water moderator. The neutron energy is calculated based on the flight time, a 20.28 m flight path length, and a 523 ns delay time after the T_0 pulse, generated when the proton bunch hits the tungsten target.

A major goal of the measurement is to obtain the ^{236}U(n,γ) cross section with improved uncertainties (less than 3%) for the incident neutron energy range from 1 keV up to 1 MeV. A detailed description of the experimental facility can be found elsewhere [18]. The new DAQ is described in Ref. [15].

In the experiment we used several different targets with different thicknesses and isotopic compositions of ^{236}U and ^{235}U to implement the ratio method described in [14, 19]. The 2013 measurement was performed using a highly enriched (over 99.9%) ^{236}U target and the 2014 measurement was performed using the mixed targets described below. The measurements are described in detail in the following sections.

A. Experiments of 2013 Beam Cycle

Most of the data were acquired with the highly enriched target. Targets used in those measurements have the following parameters:

- Target-1: A highly enriched (above 99.9%) ^{236}U target was used for most of the beam time. The target mass was about 10 mg/cm^2, which gives sufficient counting statistics for the high precision data. The target was composed of metallic granules sandwiched in between two kapton tapes.
- Target-2: The second measurement used a mixed target with the following composition of uranium isotopes: ^{236}U (80%), ^{235}U (16%) and ^{238}U (4%). The purpose of this measurement was to validate the ratio method with the different reaction rates of $N_{n,\gamma}(^{236}\mathrm{U})/N_{n,\gamma}(^{238}\mathrm{U})$ and $N_{n,\gamma}(^{236}\mathrm{U})/N_{n,f}(^{235}\mathrm{U})$. The target mass was fabricated by stippling the mixed solution on a titanium foil.
- A ^{208}Pb target was used for the neutron scattering background determination.

In this paper, we only used the highly enriched Target-1 data for the cross section determination. Target-2 data was used for the different purpose of developing a new data analysis technique to identify reaction rates from different isotopes. The new analytical technique, Independent Component Analysis, for the blind source separation is discussed in Ref. [20].

B. Experiments of 2014 Beam Cycle

The ^{236}U(n,γ) experiment continued in the 2014 beam cycle using two new targets fabricated in house. Major motivations to continue the experiments from 2013 included: (i) Reducing uncertainty in the background subtraction introduced by the 3 different uranium isotopes in Target-2 used in the 2013 experiment; (ii) Improving statistical uncertainties in the cross section determination based on the measurements taken during different beam cycles with different targets. We could add those data measured independently to increase counting statistics and reduce statistical uncertainty; (iii) Implementing a new and improved data acquisition system for further DANCE measurements. Testing the performance of new DAQ comparing the old and new data was of interest to subsequent experiments.

Targets were prepared using highly enriched (above 99.9%) ^{236}U and ^{235}U raw materials mixed in solutions with isotopic compositions shown in Tab. I. Using the same solution we produced two targets:

- Target-3: Stippled target with a mass of about 10 mg/cm^2 to measure the ratio of the ^{236}U(n,γ) and ^{235}U(n,f) reaction rates.
- Target-4: Thin electroplated target with a mass of 100 μg/cm^2 to define the absolute scale of the cross section.

The exact mass of the targets are not required as we are interested in the ratio of the two reaction rates. The isotopic composition was determined with a mass spectrometric method and shown in Tab. I.

TABLE I. Isotopic compositions in percent of the targets used in this work determined by mass spectroscopy.

Target Name	Target Mass	^{234}U	^{235}U	^{236}U	^{238}U
Target-1	20.4 mg	-	-	99.99(1)	-
Target-2	10 mg	0.0088	0.964	80.62	18.40
Target-3	10 mg	0.1120(5)	9.77(2)	89.57(4)	0.546(2)
Target-4	100 μg	0.1120(5)	9.77(2)	89.57(4)	0.546(2)

The experiments with Target-3 and Target-4 measure the rates of ^{236}U(n,γ), ^{235}U(n,γ) and ^{235}U(n,f) reactions. In our previous work [19], we confirmed that the DANCE data reduction cut on cluster multiplicity $M_{Cl} \geq 7$ was consistent with the PPAC fission fragment detector data. In other words, the high multiplicity data has a negligible contribution from neutron capture and background events unless there is pile-up.

III. DATA ANALYSIS

The timing and energy calibrations are the first step of the analysis. The primary energy calibration of the detectors was performed by measuring γ rays from the standard radioactive sources ^{22}Na, ^{60}Co and ^{88}Y. Small gain shifts were observed in the light output of each crystal during the course of the experiment, presumably due to temperature changes in the scintillators. Since barium and radium are chemical homologous, the BaF_2 crystals always contain radioactive isotopes from the radium decay chain, which turned out to be an advantage. The BaF_2 scintillation exhibits pulse shape discrimination properties and one can discriminate γ rays from α particle events. The energies of α particles emitted from these radioactive isotopes are used to update the gain for each crystal and for each run.

The DANCE array consists of 160 BaF_2 scintillator crystals in a closed 4π geometry. The BaF_2 crystal has fast (0.6 ns) and slow (600 μs) scintillation light output components. The fast timing of the scintillators leads to a precise determination of the neutron time-of-flight and a good identification of coincident γ rays following neutron capture. The high detection efficiency enables the separation of events by the Q-value of the reaction while the high detector segmentation of DANCE enables measurement of the γ-ray multiplicity distribution. These features of DANCE help to improve the signal-to-noise ratio by gating on the γ-ray multiplicity and the total γ-ray energy around the ^{236}U(n,γ) reaction Q-value, 5.12 MeV. Fig. 2 illustrates the selection of the appropriate cut that gives high enough counting statistics as well as low background. Actual data reduction cuts for the cross section analysis will be discussed later.

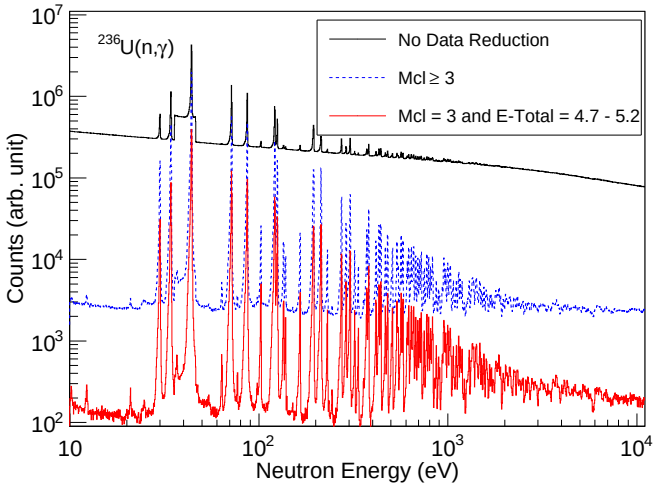

FIG. 2. Neutron time-of-flight spectrum of the ^{236}U(n,γ) measurement with the highly enriched Target-1.

A. Background Subtraction

There are several types of background in DANCE experiments, as discussed in Ref. [21] in detail. The constant background from intrinsic α-activities of BaF_2 crystal is easily suppressed using pulse shape discrimination (PSD) of the waveforms [18]. Events from β-activities are suppressed by setting the total γ-ray energy cut above 3 MeV. In the same way, the total γ-ray energy cut can also eliminate background due to γ-rays in the beam. These γ rays originate mainly from the neutron production area and have energies below 3 MeV [21].

The Q-values of the radiative capture reactions on ^{236}U and ^{235}U isotopes are 5.125 and 6.545 MeV, respectively. Thus the contribution from the ^{235}U(n,γ) and ^{235}U(n,f) reactions can not be separated by the total energy cut perfectly. We used the highly enriched ^{235}U (HEU) data to subtract the ^{235}U contributions for the mixed target measurements.

The data reduction cut, *cut1*, was set for cluster multiplicity $M_{Cl} = 3$ and 4 and total γ-ray energy $E_{Total} =$ 4.6 to 5.2 MeV.

$$N_{n,\gamma}(E_n) = [N_{U236/5}(E_n) - \alpha N_{235U}(E_n)] - \beta N_{208Pb}(E_n), \quad (1)$$

where $N_{U236/5}(E_n)$ are the counts from Target-3 or Target-4 data within the *cut1*, $N_{235U}(E_n)$ and $N_{208Pb}(E_n)$ are highly enriched ^{235}U and ^{208}Pb targets respectively within the *cut1*.

The bin-by-bin normalization coefficient α, was obtained by taking the ratio of counts within the cuts for $M_{Cl} \geq 7$ and the total γ-ray energy from 3 MeV to 15 MeV, *cut2*. The integration region is shown in the bottom panel of the Fig. 3 with a red rectangle. The coefficients α and β are:

$$\alpha = \frac{N^{cut2}_{U236/5}}{N^{cut2}_{U235}} \quad \text{and} \quad \beta = \frac{N^{cut3}_{U236/5}}{N^{cut3}_{Pb208}}$$

where α should be zero for the Target-1 data because it has no contribution from ^{235}U. The normalization coefficient β is related to the scattering background. Neutrons scattered from the target can be captured by the Ba isotopes in the detector crystals and produce γ rays. In order to reduce this background, a ^{6}LiH shell of 6-cm thickness surrounds the target. Despite the absorbing effects of the ^{6}LiH shell, some neutrons scattered by the target reach the detector.

As illustrated in the top panel of Fig. 3, the bin-by-bin normalization coefficient α

is determined by the ratio of events cut on the total γ-ray energy around the Ba capture peaks. The cut used for the scattering background normalization was set to $M_{Cl} = 3$ and 4 and $E_{Total} = 7.5$ MeV to 9.2 MeV, *cut3*.

The capture γ rays from the target, located at the center of DANCE, are emitted into a 4π solid angle and typically create several clusters of fired BaF_2 detectors. On the other hand, the capture of the scattered neutrons occurs in the BaF_2 crystals and usually creates only a few clusters. Therefore the low cluster multiplicity spectra have a high background contribution from the capture of the scattered neutrons, while smaller background is observed at multiplicities $M_{Cl} > 2$.

Finally, delayed fission γ rays can contribute to a background for fissile target measurements as described in Ref. [22]. In the ^{236}U case, the fission cross section is negligible compared to the capture cross section, and it increases above 800 keV incident neutron energy.

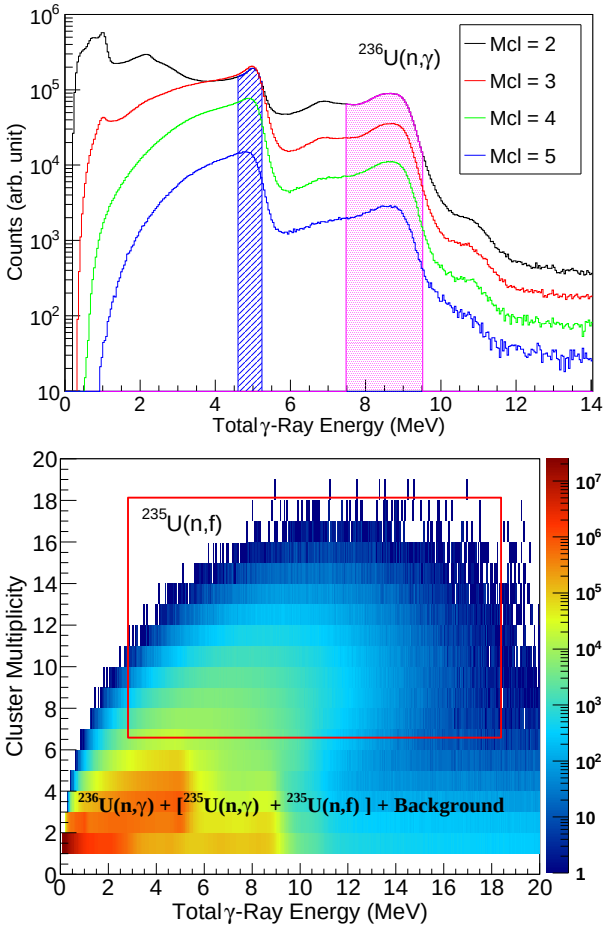

FIG. 3. Top panel, total γ-ray energy spectra at different multiplicities. The highlighted areas show the *cut1* and *cut3*. Bottom panel, ^{235}U Fission events. Red square shows the *cut2*.

IV. CROSS SECTION DETERMINATION

Neutron induced (n,γ) or (n,f) cross sections can be determined from the following formula

$$\sigma_{n,\gamma/n,f}(E_n) = \frac{A}{N_A m} \frac{N_{n,\gamma/n,f}(E_n)}{\varepsilon_{n,\gamma/n,f}\Phi(E_n)S}, \quad (2)$$

where A, N_A and m are atomic mass, Avogadro's number and areal density of the targets, respectively. $N_{n,\gamma/n,f}(E_n)$ is the measured yield after the background subtraction, $\varepsilon_{n,\gamma/n,f}(E_n)$ is the efficiency of the detection for a given data reduction cut and $\Phi(E_n)$ and S are the beam flux and illuminated target area.

The beam flux and the target areal density are not homogeneous. Their absolute values can be determined with large uncertainties. Therefore, the neutron capture cross section can be obtained relative to a the well known calibration standard as ^{197}Au [23] for example. A novel approach was introduced in our recent publication [14, 19] using the ^{235}U(n,f) cross section as a reference. The ^{236}U(n,γ) and ^{235}U(n,f) reaction rates are measured simultaneously with the Target-3 experiment. The ratio of the two reaction rates is proportional to the ratio of the corresponding cross sections, detection efficiencies and isotopic compositions. The capture cross section relative to the fission cross section is defined as:

$$\sigma_{n,\gamma}(E_n) = A_{n,\gamma}(E_n) \frac{N_{n,\gamma}(E_n)}{N_{n,f}(E_n)} \sigma_{n,f}(E_n), \quad (3)$$

where

$$A_{n,\gamma}(E_n) = \frac{\varepsilon_{n,f}}{\varepsilon_{n,\gamma}} R_{235U/236U}, \quad (4)$$

$\varepsilon_{n,f}$ and $\varepsilon_{n,\gamma}$ are the efficiencies for detecting (n, f) and (n, γ) events, respectively. $R_{235U/236U}$ is the ratio of the isotopic compositions in the target.

The normalization constant shown in Eq. (4) is assumed to be independent of incident neutron energy and is calculated with numerical values of the parameters given in the Tab. I and Sec. V C. Using the Target-4 data, the absolute value of the ^{236}U(n, γ) cross section for the resonances at 5.45 eV and 43.91 eV is determined relative to the ^{235}U(n, f) cross section at 8.76 eV and 35.18 eV using the Eqs. (3) and (4). Since the reference fission resonance is at different incident neutron energy than the capture resonance, the reaction rates were normalized to the neutron flux measured with a ^{6}Li neutron flux monitor. The neutron flux at low energy is large, and the statistical uncertainty of the flux normalization coefficients is small. The final result of the cross section is determined from the Target-1 and Target-3 data normalized to the absolute value of the cross section from the Target-4.

V. THE EXPERIMENTAL CONSIDERATIONS

There are several experimental effects that have to be considered carefully for accurate cross section determination. Some of these corrections are relatively simple to calculate, while some of them require complex calculations. We used the R-Matrix data analysis tool SAMMY [24] that is well known in the experimental nuclear physicists community for the corrections in Sec. V A and V B. The corrections are discussed below.

A. Self shielding and multiple scattering

We need to estimate self shielding and multiple scattering corrections before we determine cross sections with the ratio method for two independent measurements with different targets. The self shielding correction could be calculated analytically with a relatively simple formula. We used the SAMSMC Monte-Carlo code to estimate single and multiple scattering corrections. Inputs for the code are the sample geometry, isotopic composition and beam area. Other important inputs are capture and total cross section taken from the ENDF/B VII.1 database. The corrections are larger as the sample thickness increases. With simulations for the Target-3 geometry, we estimated up to 10% corrections for the strongest resonance at 5.3 eV, and they were much smaller than 5% for the weaker resonances. The estimated correction was less than 0.1% for the region of incident neutron energy above 1 keV. For the resonance parameters below 1 keV, self shielding and multiple scattering corrections were included in the SAMMY fitting.

B. Resolution broadening

Depending on the spallation target and the moderator geometries, the conversion of flight time to energy of the neutrons hitting the target nuclei is determined with some uncertainty or so-called resolution broadening. The SAMMY code has several choices of analytical expressions for the broadening function dedicated to specific facilities. We used the RPI broadening function with the parameters adjusted for the DANCE flight path using well known ^{197}Au resonances by P. E. Koehler [25].

The analytical expression of the resolution function cannot fully describe the low energy tail of the resonances. Corrections in the unresolved resonance region cannot be made with the SAMMY code. For those reasons, we have made a Monte-Carlo simulation to reproduce the broadened energy distributions [26]. The broadening function is typically neutron energy-dependent and its time-dependent numerical matrix was quantified using Monte Carlo simulations. The inverse problem to convert Time-of-Flight to the broadened neutron energy is in progress and not included in this paper.

C. γ Ray detection efficiency

The detection efficiency is one of the most important characteristics of the detector system. Not all γ rays emitted by the target and passing through DANCE will produce a count. The probability a γ ray will interact with the detector and produce a count is the efficiency of the detector:

$$\varepsilon_{n,\gamma/n,f} = \frac{\text{Detected counts within the cuts}}{\text{Total number of capture/fission events}} \quad (5)$$

The single γ-ray efficiency is determined with standard γ-ray sources whose activities are known. It is essential to know the detector response functions for γ-rays with different energies and multiplicities. GEANT4 simulations of the DANCE array were in good agreement with experiments performed with calibration sources.

We used the same technique for the efficiency estimation as described in Ref. [23].

Fig. 4 shows the spectra for the γ-ray detection efficiency. The efficiency $\varepsilon_{n,\gamma}$ is estimated as the ratio of counts in the red areas (total γ ray energy gate) of the multiplicity $M_{Cl} = 3$ and 4 ($cut1$) spectra to the total counts observed (no total γ ray energy gate) summed over $M_{Cl} = 1$ to 7 spectra.

The fission efficiency, $\varepsilon_{n,f}$, is estimated from the earlier PPAC fission tagging detector measurement on highly enriched ^{235}U data. It is calculated with the ratio of high multiplicity ($cut3$) yields to the counts in multiplicity all,

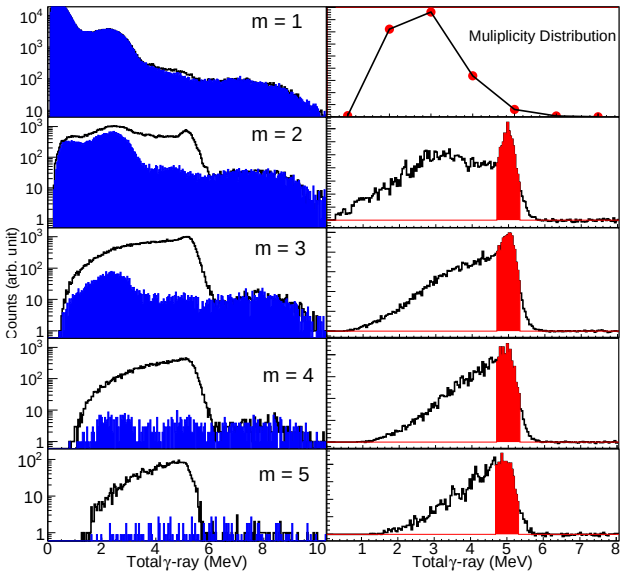

FIG. 4. Total γ-ray spectra gated on a neutron resonance at 43.91 eV. Left column: the total γ-ray energy spectrum at the resonance (solid line) and in the valley between the resonances (blue stippled area) used for the background subtraction. Right column: The spectrum after the subtraction of the background (solid line) and the total γ-ray energy cut applied for the analysis. The multiplicity distribution based on the counts within the cuts are shown in the top panel of the right column.

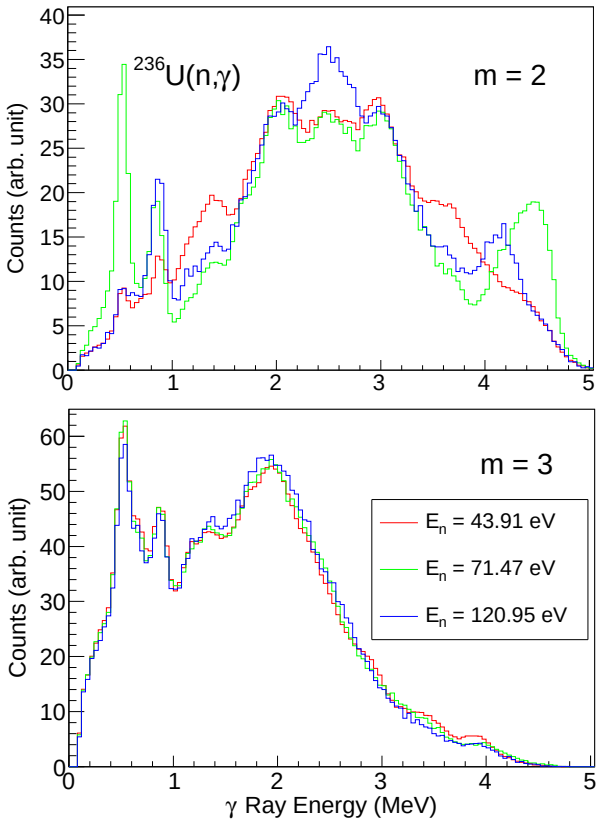

FIG. 5. Multi step cascade spectra and the multiplicity distribution of all observed strong resonances.

$M_{Cl} = 1$ to 20. We confirmed that Target-3 and Target-4 data within the *cut*3 were consistent with the PPAC data with the relative normalization. In summary, the capture efficiency for the *cut*1 is $\varepsilon_{n,g} = 15.7\%$ and the fission efficiency for cut3 is $\varepsilon_{n,f} = 31.9\%$.

D. Radiation widths fluctuations and detector response

In the statistical model of nuclear reactions, the radiative decay pattern depends on the level density, spin distribution and the radiative strength function of the nuclei. The s-wave resonances of the even-even ^{236}U nuclei have the same spins ($I = 1/2^+$), and the multiplicity distributions for all s-wave resonances are similar to each other with small fluctuations. The fluctuations are due to the Porter-Thomas fluctuations of the partial radiation widths.

Multi step cascade γ-ray energy spectra from the s-wave resonances at $E_n = 43.91$ eV, $E_n = 71.47$ eV and $E_n = 120.95$ eV are shown in Fig. 5. These spectra are similar for all s-wave resonances despite the fluctuations in low-energy transitions. Carpenter and Bollinger [27] showed that there is a strong correlation between total radiation width, Γ_γ, and the fluctuations of a few strong transitions to the final state at low energy. The fluctuations lead to a small difference in multiplicity distribution for the resonances at different energies. Depending on the selection of the total γ-ray energy cut, a systematic uncertainty due to the fluctuations would be expected. Detailed analysis of the radiative decay properties on Uranium isotopes will be published in a separate work [28].

Fig. 6 shows average multiplicities calculated for the stronger low-energy resonances up to 700 eV with different thresholds and coincidence windows. For DANCE, the γ-ray detection threshold is about 100 to 200 keV. One would expect that the detection efficiency and the multiplicity distribution change depending on the threshold. The difference will be larger if there is a non-negligible amount of low-energy transitions within the cascade. The average multiplicity changes systematically for different settings of the software threshold at 100 and 150 keV. The final results are reported for the data with 100 keV threshold.

The data analysis software builds the capture event based on a coincidence signal within a specific coincidence window. The radiative time is usually very fast, femtoseconds, for most of the transitions. It is also possible that the transition time to the ground state takes longer than several nanoseconds if there is a metastable state populated within the cascade. There are two

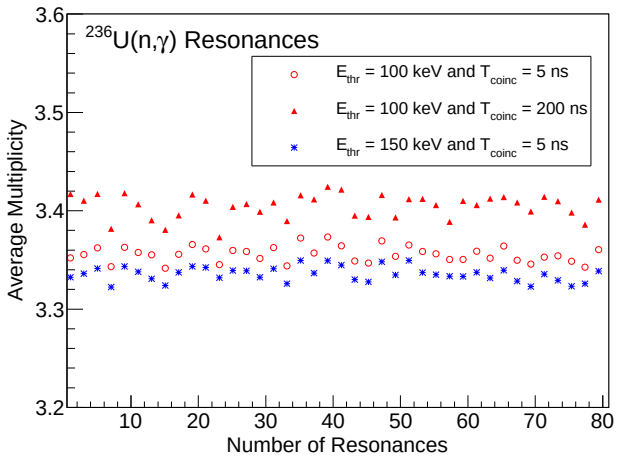

FIG. 6. Average multiplicity of the resonances with different thresholds and coincidence windows. The resonance number corresponds to energy orderings in Tab. II.

metastable states indicated in ^{237}U level scheme at 159.96 keV (3.2 ns) and 274.0 keV (155 ns). Populations of those metastable states are probably very weak and the multiplicity distribution were almost the same for the coincidence window settings of 5 ns and 200 ns.

Just as there are fluctuations in the average multiplicity, the γ-ray detection efficiency, $\varepsilon_{n,\gamma}$, also changes both with the selection of cuts and resonances to resonance. If we calculate the cross section with selected cuts and efficiency, we would expect a small fluctuation. The maximum systematic uncertainty related to the efficiency fluctuation is estimated to be about 1.7%.

VI. RESULTS

The absolute scale of the cross section is set according to the thin target measurement as explained in Sec. IV. The integrated ^{235}U(n,f) cross sections of 152.5(9) eVb within the range from 8.59 eV to 9.03 eV and 283.3(21) eVb within the range from 34.20 eV to 35.98 eV are used as reference cross sections for the ^{236}U(n,γ) resonances at 5.45 eV and 43.91 eV, respectively. The integrated cross section of the ^{236}U resonance at energy range from 5.35 eV to 5.57 eV was determined as 1331(8) eVb from Eq. (3) and (4) which is compared to 1386(2) eVb, ENDF/B-VII.1 and 1340 eVb, JEFF-3.1. The self shielding correction is estimated to be about 1.9% for the 5.45 eV resonance, which increased the measured cross section to 1356(8) eVb. The capture cross section at the range from 43.05 eV to 44.46 eV was determined as 753(20) eVb compared to 642(12) eVb, ENDF/B-VII.1 and 833 eVb, JEFF-3.2.

The ^{236}U(n,γ) reaction rates from the Target-1 data and the ^{235}U(n,f) reaction rate from the independent measurement with the highly enriched uranium target are also used to determine the cross section in the unresolved resonance region. The results from the two different data sets were consistent within the statistical uncertainty.

The main goal of the experiments was a high precision cross section from 1 keV to 1 MeV incident neutron energy region. We report the results in two separate regions discussed below. High resolution was used to obtain the resonance parameters for the resolved resonance region. To increase the counting statistics above 1 keV, wide bins were used.

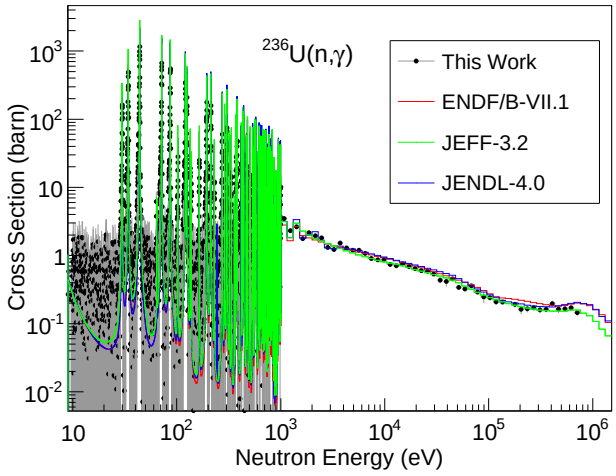

FIG. 7. ^{236}U Neutron Capture Cross Section.

A. Resolved resonance region

The cross section values in the resonance region were used in the determination of neutron, Γ_n, and total radiative widths, Γ_γ using the multilevel R-matrix code SAMMY [24]. Doppler broadening, the DANCE flight path timing resolution broadening function, target self-shielding, and multiple scattering corrections were taken into account during the data fitting. The RPI resolution broadening function with coefficients adjusted for DANCE flight path was used [25].

It is hard to extract both Γ_n and Γ_γ at the same time without any transmission data. However the widths can be obtained from the capture data for strong, low energy resonances where the incident neutron energy resolution makes it possible to exploit the detailed resonance shape. For high incident neutron energy, above several hundreds of eV for DANCE flight path, the shape of the resonance is dominantly broadened by the resolution function. In this cases, SAMMY essentially extracts the area under the resonance as a function of Γ_n and Γ_γ. Therefore, SAMMY produces relatively large uncertainties to the resonance parameters when fitting both of them as a variable. The components of resonance parameter uncer-

tainty were experimental, resolution function, time zero, sample thickness, burst width and flight path length. They were propagated into resonance energy and neutron width uncertainties through use of the Propagated Uncertainty Parameters (PUP) feature in SAMMY.

Neutron and radiation widths for the resonances up 1 keV are listed in Tab. II. The values given in Tab. II are obtained from the SAMMY output file SAMMY.PUB that is formatted for publication containing resonance parameter values and their uncertainties. The neutron and radiation widths obtained from our measurement agree well within experimental errors with the previously published ENDF values. The resonances above 1 keV become very broad because of the energy resolution.

Average resonance parameters can be obtained from the information given in Tab. II using the analytical technique stated in Ref. [29]. Most of the experimentally observed resonances are s-wave and due to PT fluctuations, some resonances are weak and experimentally unobservable. The cumulative plot of the number of observed resonances as a function of neutron energy gives a hint of missing resonances. The cumulative plot starts deviate from a straight line at above 300 keV which indicates an increasing number of missing levels, but they may be an artifact of statistical fluctuations. We estimate the fraction of missing strength at a maximum of about 2% below the 250 eV neutron incident energy. The estimate of average parameters are thus, reasonable, as the missing strength is much smaller than the uncertainty arising from the PT distribution itself as well as from the experimental uncertainty. Average level spacing of the s-wave resonances up to 250 eV was about $D_0 = 14.3 \pm 0.2$ eV and for the long range up to 1 keV, it was about $D_0 = 17.3 \pm 0.1$ eV.

TABLE II: The resonance parameters for ^{236}U isotopes.

ENDF-B/VII.1				This Work		
E_n (eV)	J	Γ_γ (meV)	Γ_n (meV)	E_n (eV)	Γ_γ (meV)	Γ_n (meV)
29.8	1/2	19.5	0.551	29.865(2)	18.6(17)	0.52(3)
34.1	1/2	19.5	2.37	34.133(2)	21.8(16)	1.63(3)
43.91	1/2	21.0	25.7	43.891(2)	14.6(1)	27.0(14)
64.28	1/2-	19.5	0.036	63.51(5)	19.8(10)	0.0364(6)
71.47	1/2	23.1	19.6	71.439(3)	17.4(15)	14.4(11)
-	1/2-	-	-	76.85(4)	19.1(17)	0.329(9)
86.51	1/2	22.6	28.3	86.457(4)	15.7(9)	24.8(22)
102.3	1/2	19.5	0.597	102.203(3)	18.2(12)	0.55(6)
120.95	1/2	22.0	48.3	120.847(3)	16.6(16)	47.7(42)
124.88	1/2	19.7	17.2	124.817(4)	17.8(12)	15.3(20)
134.57	1/2	19.5	0.906	134.450(2)	19.5(18)	0.90(9)
137.76	1/2	19.5	0.497	137.646(3)	19.4(18)	0.49(5)
164.72	1/2	19.5	1.754	164.617(4)	19.5(18)	1.8(2)
192.89	1/2	19.0	3.628	192.594(2)	19.1(18)	3.6(4)
194.35	1/2	20.0	46.0	194.166(6)	20.4(20)	46(4)
212.75	1/2	23.9	86.6	212.57(2)	18.9(17)	73(7)
229.63	1/2	19.5	1.724	230.09(1)	19.3(19)	1.7(2)
272.93	1/2	22.9	30.7	272.79(3)	14.4(12)	22.4(23)
288.68	1/2	25.0	10.77	288.519(4)	24.9(25)	10.7(11)
303.15	1/2	23.6	78.5	302.96(4)	21.5(17)	72.3(71)
320.5	1/2	19.5	4.66	320.309(2)	19.3(19)	4.6(5)

TABLE II – continued from previous page

ENDF-B/VII.1				This Work		
E_n (eV)	J	Γ_γ (meV)	$g\Gamma_n$ (meV)	E_n (eV)	Γ_γ (meV)	Γ_n (meV)
334.96	1/2	19.5	4.97	334.695(2)	19.5(20)	5.0(5)
371.18	1/2	24.0	12.66	370.828(4)	24.0(24)	12.7(13)
379.8	1/2	20.0	93.1	379.46(1)	19.6(19)	88.3(88)
415.39	1/2	16.7	15.52	415.117(4)	16.6(17)	15.4(16)
430.95	1/2	20.1	57.2	430.59(2)	19.6(20)	56.2(56)
440.63	1/2	22.1	60.1	440.021(7)	22.0(21)	59.7(59)
466.5	1/2	17.0	14.08	464.575(5)	17.0(17)	14.1(14)
478.39	1/2	18.9	36.38	478.15(1)	19.5(19)	37.4(36)
500.4	1/2	19.5	2.155	500.43(4)	19.5(19)	2.15(22)
507.1	1/2	16.2	17.667	506.581(5)	16.1(16)	17.6(20)
536.4	1/2	17.6	29.389	536.11(1)	17.4(18)	29.1(29)
542.8	1/2	13.6	9.165	542.652(3)	13.6(14)	9.16(92)
564.4	1/2	21.1	77.4	563.215(9)	20.9(21)	76.5(77)
576.2	1/2	22.8	152.0	575.53(3)	22.2(22)	148.6(98)
607.1	1/2	15.4	13.143	606.144(3)	15.4(15)	13.1(13)
617.8	1/2	20.7	42.493	616.819(7)	20.5(21)	42.1(42)
637.8	1/2	20.9	65.16	637.19(1)	20.8(21)	64.8(64)
647.6	1/2	18.7	6.029	646.90(1)	18.7(19)	6.0(6)
655.6	1/2	23.0	93.107	654.45(1)	21.8(22)	88.4(90)
673.6	1/2	19.6	48.587	673.13(2)	19.5(20)	48.3(48)
691.3	1/2	18.8	29.127	690.58(3)	18.8(19)	29.1(29)
706.0	1/2	21.0	28.841	705.105(8)	21.0(21)	28.8(29)
720.6	1/2	20.1	97.361	719.87(1)	20.1(20)	97.4(97)
746.3	1/2	17.5	20.073	745.485(7)	17.5(18)	20.1(20)
770.7	1/2	22.0	184.34	769.65(3)	21.7(22)	182.0(98)
789.4	1/2	20.7	81.227	788.28(2)	20.6(21)	80.7(81)
806.6	1/2	20.0	37.075	805.692(8)	20.0(20)	37.0(4)
820.3	1/2	12.3	7.378	820.156(6)	12.3(12)	7.4(7)
827.4	1/2	28.0	109.48	826.93(7)	27.9(28)	109.2(84)
864.9	1/2	17.1	16.537	864.11(1)	17.1(17)	16.5(16)
888.8	1/2	19.5	8.164	883.570(5)	19.5(20)	8.15(81)
900.4	1/2	19.5	6.332	899.19(2)	19.5(20)	6.33(63)
930.7	1/2	15.7	7.31	929.471(5)	15.7(16)	7.31(73)
948.5	1/2	24.0	157.21	945.99(2)	24.0(24)	157(15)
955.2	1/2	18.8	36.367	953.60(2)	18.8(19)	36.3(36)
969.3	1/2	23.0	315.5	968.11(2)	23.2(22)	317(31)
994.7	1/2	22.0	151.99	993.5(1)	22.0(22)	152(15)
998.1	1/2	13.7	8.974	998.69(1)	13.7(14)	9.0(9)

B. Unresolved Region

Figure 7 shows the result of the cross section obtained using the reaction rate ratios of $^{238}\mathrm{U}(n,\gamma)$ and $^{235}\mathrm{U}(n,f)$. Here we combined all experimental yields from 2013 to 2015 since the data were consistent with each other within their statistical uncertainty.

As it is shown in Fig. 1, cross sections from the Bergman and Adamchuk experiments as well as our results agree well with the nuclear data evaluations for the incident neutron energy range from 1 keV to about 20 keV. Between about 50 keV and 100 keV, there is only one set of experimental data, measured by Kazakov *et al.* It is consistent with our results. Above 100 keV, the previous experimental data have big discrepancies and the ENDF/B-VII.1 and JEFF-3.2 evaluations are different. Our result agree better with the JEFF-3.2 evaluation.

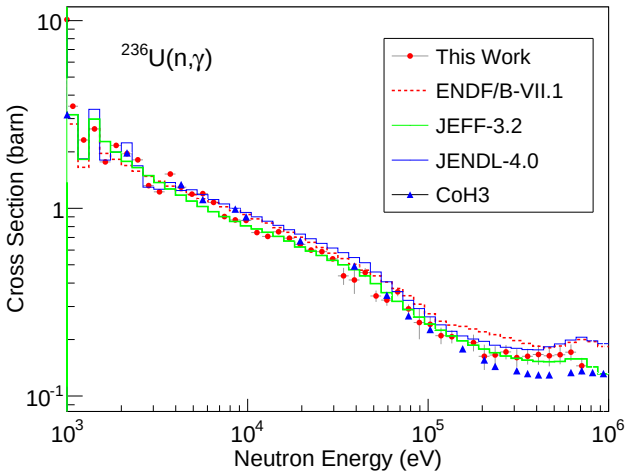

FIG. 8. ^{236}U Neutron Capture Cross Section in Unresolved Resonance Region Compared with the Theoretical Calculation.

The Hauser-Feshbach model calculation of the $^{236}\mathrm{U}(n,\gamma)$ cross section is shown in Fig. 8.

We performed a statistical Hauser-Feshbach model calculation for the neutron-induced reaction on ^{236}U with the coupled-channels Hauser-Feshbach code $\mathrm{CoH_3}$ [30]. The nuclear deformation parameters were taken from the Finite-Range Droplet Model (FRDM) [31], and five levels in the ground state rotational band, 0^+, 2^+, 4^+, 6^+, and 8^+, were coupled. $\mathrm{CoH_3}$ includes the width fluctuation correction of Moldauer [32, 33], with the so-called Engelbrecht-Weidenmüller transformation that is a strict treatment of the directly coupled channels in the Hauser-Feshbach theory [34, 35]. We employed the coupled-channels optical potential of Soukhovitskii *et al.* [36].

The most important model parameters in the neutron capture calculation are the level density and the γ-ray strength functions, assuming the compound formation cross section given by the coupled-channels calculation is reasonable. The level density of ^{237}U was calculated with the Gilbert-Cameron formula [37, 38], in which the constant temperature model is adopted at low excitation energies, and the Fermi gas model at higher energies. The level density parameter was adjusted a few percent to reproduce the reported s-wave average resonance spacing D_0 of 14 eV [39]. We examined a parity dependence of the D_0 by calculating a combinatorial level density based on the single-particle states of FRDM [31], and confirmed that there is no significant difference in the numbers of even and odd parity states at the neutron separation energy.

To calculate the γ-ray transmission coefficients, we adopted the generalized Lorentzian form of Kopecky and Uhl [40] for the $E1$ giant dipole resonance (GDR), with the GDR parameters taken from RIPL-3 [39, 41]. We also included the standard Lorentzian profile for the $M1$ spin-flip mode and $E2$, with the systematic study on GDR in RIPL-3 [39]. In addition to these γ-ray strengths, we considered the $M1$ scissors mode [42]. Although the fission cross section is negligible in the energy range of our interest, the fission barrier parameters were taken from the values adopted in JENDL-4 [43], and slightly adjusted to the evaluated fission cross sections.

VII. SUMMARY

The cross section of $^{236}\mathrm{U}(n,\gamma)$ reaction for neutron energies from 10 eV to 800 keV was measured with the DANCE calorimeter at the Los Alamos Neutron Science Center using the time-of-flight method. The result agrees with current nuclear data evaluation below 10 keV incident neutron energy. It agrees better with the JEFF-3.2 nuclear data, and it was systematically lower than the ENDF-B/VII.1 evaluation about 15% to 20% above 100 keV.

Individual resonance parameters, radiation and neutron widths, were determined with the SAMMY code. Analysis of the fit results yielded an s-wave strength function of 10^3 $\mathrm{S_0} = 2.58 \pm 0.30$ eV and an average total radiative width of $\Gamma_\gamma = 19.3 \pm 1.8$ meV. These numbers are in agreement with the previous experiments and ENDF-B/VII.1 library parameters.

ACKNOWLEDGMENTS

This work was performed under the auspices of the U.S. Department of Energy by Los Alamos National Security, LLC, under contract DE-AC52-06NA25396. This work benefited from the use of the LANSCE accelerator facility. This work has been supported by the U.S. Department of Energy, Office of Science, Nuclear Physics under the Early Career Award No. LANL20135009.

[1] V. G. Pronyaev, *Assessment of Nuclear Data Needs for Thorium and other Advanced Cycles*, Tech. Rep. INDC(NDS)-408 (International Atomic Energy Agency, 1999).
[2] M. H. V. M. Maslov, P. Oblozinsky, *Review and Assessment of Neutron Cross Section and Nubar Covariances for Advanced Reactor Systems*, Tech. Rep. BNL-81884-2008-IR (Brookhaven National Laboratory, 2008).
[3] P. Hubert, R. Joly, and G. Vendryes, Comptes Rendus **241**, 392 (1955).
[4] B. V. Efimov and J. I. Mityaev, Atomnaya Energiya **1**, 130 (1956).
[5] J. F. Barry, J. L. Bunce, and J. L. Perkin, Proceedings of the Physical Society (London), **78**, 801 (1961).

[6] D. C. Stupegia, R. R. Henrich, and G. H. Mccloud, J. Nuclear Energy AB (Reactor Sci. and Technol.) **15**, 200 (1961).

[7] J. A. Harvey and D. J. Hughes, Phys. Rev. **109**, 471 (1958).

[8] R. L. Macklin and C. W. Alexander, Nucl. Sci. Eng. **104**, 258 (1990).

[9] A. D. Carlson, S. J. Friesenhahn, W. M. Lopez, and M. P. Fricke, Nuclear Physics, Section A **141**, 577 (1970).

[10] F. Gunsing, S. Andriamonje, E. Berthoumieux, A. Borella, W. Dridi, G. Aerts, J. Pancin, L. Perrot, A. Plukis, P. Schillebeeckx, and et al., "Measurement of the neutron capture cross section of sup 236u," (American Nuclear Society - ANS; La Grange Park (United States), 2006) p. (B072), advances in Nucl.Analysis and Simul.,Vancouver, 2006.

[11] M. Barbagallo, N. Colonna, M. Vermeulen, S. Altstadt, J. Andrzejewski, L. Audouin, V. Bcares, F. Bev, F. Belloni, E. Berthoumieux, J. Billowes, V. Boccone, D. Bosnar, M. Brugger, M. Calviani, F. Calvio, D. Cano-Ott, C. Carrapio, F. Cerutti, E. Chiaveri, M. Chin, G. Corts, M. Corts-Giraldo, M. Diakaki, C. Domingo-Pardo, I. Duran, R. Dressler, C. Eleftheriadis, A. Ferrari, K. Fraval, S. Ganesan, A. Garca, G. Giubrone, I. Gonalves, E. Gonzlez-Romero, E. Griesmayer, C. Guerrero, F. Gunsing, A. Hernndez-Prieto, D. Jenkins, E. Jericha, Y. Kadi, F. Kppeler, D. Karadimos, N. Kivel, P. Koehler, M. Kokkoris, M. Krtika, J. Kroll, C. Lampoudis, C. Langer, E. Leal-Cidoncha, C. Lederer, H. Leeb, L. Leong, R. Losito, A. Mallick, A. Manousos, J. Marganiec, T. Martnez, C. Massimi, P. Mastinu, M. Mastromarco, E. Mendoza, A. Mengoni, P. Milazzo, F. Mingrone, M. Mirea, W. Mondalaers, C. Paradela, A. Pavlik, J. Perkowski, A. Plompen, J. Praena, J. Quesada, T. Rauscher, R. Reifarth, A. Riego, M. Robles, C. Rubbia, M. Sabat-Gilarte, R. Sarmento, A. Saxena, P. Schillebeeckx, S. Schmidt, D. Schumann, G. Tagliente, J. Tain, D. Tarro, L. Tassan-Got, A. Tsinganis, S. Valenta, G. Vannini, V. Variale, P. Vaz, A. Ventura, V. Vlachoudis, R. Vlastou, A. Wallner, T. Ware, M. Weigand, C. Wei, T. Wright, and P. ugec, Nuclear Data Sheets **119**, 45 (2014).

[12] G. V. Muradyan, Atomnaya Energiya **110**, 100 (2011).

[13] M. Heil, R. Reifarth, M. Fowler, R. Haight, F. Kppeler, R. Rundberg, E. Seabury, J. Ullmann, J. Wilhelmy, and K. Wisshak, Nuclear Instruments and Methods in Physics Research Section A: Accelerators, Spectrometers, Detectors and Associated Equipment **459**, 229 (2001).

[14] Jandel, M., Baramsai, B., Bond, E., Rusev, G., Walker, C., Bredeweg, T. A., Chadwick, M. B., Couture, A., Fowler, M. M., Hayes, A., Kawano, T., Mosby, S., Stetcu, I., Taddeucci, T. N., Talou, P., Ullmann, J. L., Vieira, D. J., and Wilhelmy, J. B., Eur. Phys. J. A **51**, 179 (2015).

[15] Couture, A., Mosby, S., Baramsai, B., Bredeweg, T. A., Jandel, M., Macon, K., ODonnell, J. M., Rusev, G., Taddeucci, T. N, Ullmann, J. L., and Walker, C. L., EPJ Web of Conferences **93**, 07003 (2015).

[16] M. Chadwick, M. Herman, P. Obložinský, *et al.*, Nuclear Data Sheets **112**, 2887 (2011), special Issue on ENDF/B-VII.1 Library.

[17] A. Koning, C. Dean, U. Fischer, and R. Mills, The JEFF-3.1 Nuclear Data Library, JEFF Report **23** (2013).

[18] J. M. Wouters, A. A. Vicente, T. A. Bredeweg, E. Esch, R. C. Haight, R. Hatarik, J. M. O'Donnell, R. Reifarth, R. S. Rundberg, J. M. Schwantes, S. A. Sheets, J. L. Ullmann, D. J. Vieira, and J. B. Wilhelmy, IEEE Transactions on Nuclear Science **53**, 880 (2006).

[19] M. Jandel, T. A. Bredeweg, E. M. Bond, M. B. Chadwick, A. Couture, J. M. O'Donnell, M. Fowler, R. C. Haight, T. Kawano, R. Reifarth, R. S. Rundberg, J. L. Ullmann, D. J. Vieira, J. M. Wouters, J. B. Wilhelmy, C. Y. Wu, and J. A. Becker, Phys. Rev. Lett. **109**, 202506 (2012).

[20] Jandel, M., Baramsai, B., Bond, E., Rusev, G., Walker, C., Bredeweg, T. A., Chadwick, M. B., Couture, A., Fowler, M. M., Hayes, A., Kawano, T., Mosby, S., Stetcu, I., Taddeucci, T. N., Talou, P., Ullmann, J. L., Vieira, D. J., and Wilhelmy, J. B., Eur. Phys. J. A **51**, 179 (2015).

[21] R. Reifarth, T. Bredeweg, A. Alpizar-Vicente, J. Browne, E.-I. Esch, U. Greife, R. Haight, R. Hatarik, A. Kronenberg, J. O'Donnell, R. Rundberg, J. Ullmann, D. Vieira, J. Wilhelmy, and J. Wouters, Nuclear Instruments and Methods in Physics Research Section A: Accelerators, Spectrometers, Detectors and Associated Equipment **531**, 530 (2004).

[22] S. Mosby, T. A. Bredeweg, A. Chyzh, A. Couture, R. Henderson, M. Jandel, E. Kwan, J. M. O'Donnell, J. Ullmann, and C. Y. Wu, Phys. Rev. C **89**, 034610 (2014).

[23] M. Jandel, T. A. Bredeweg, E. M. Bond, M. B. Chadwick, R. R. Clement, A. Couture, J. M. O'Donnell, R. C. Haight, T. Kawano, R. Reifarth, R. S. Rundberg, J. L. Ullmann, D. J. Vieira, J. B. Wilhelmy, J. M. Wouters, U. Agvaanluvsan, W. E. Parker, C. Y. Wu, and J. A. Becker, Phys. Rev. C **78**, 034609 (2008).

[24] N. M. Larson, *Udated Users Guide for SAMMY*, Tech. Rep. ORNL/TM-9179/R7 (2006).

[25] P. E. Koehler, Private communication.

[26] M. Mockov, Private communication.

[27] tagkey1970iv, in *Experimental Neutron Resonance Spectroscopy*, edited by J. HARVEY (Academic Press, 1970) p. 308.

[28] J. L. Ullmann, T. Kawano, M. Krtička, and et al., In preparation for publication.

[29] B. Baramsai, G. E. Mitchell, U. Agvaanluvsan, F. Bečvář, T. A. Bredeweg, A. Chyzh, A. Couture, D. Dashdorj, R. C. Haight, M. Jandel, A. L. Keksis, M. Krtička, J. M. O'Donnell, R. S. Rundberg, J. L. Ullmann, D. J. Vieira, and C. L. Walker, Phys. Rev. C **85**, 024622 (2012).

[30] T. Kawano, P. Talou, M. B. Chadwick, and T. Watanabe, Journal of Nuclear Science and Technology **47**, 462 (2010).

[31] P. Möller, J. R. Nix, W. D. Myer, and W. Swiatecki, Atomic Data and Nuclear Data Tables **59**, 185 (1995).

[32] P. A. Moldauer, Nuclear Physics A **344**, 185 (1980).

[33] T. Kawano, P. Talou, and H. A. Weidenmüller, Phys. Rev. C **92**, 044617 (2015).

[34] C. A. Engelbrecht and H. A. Weidenmüller, Phys. Rev. C **8**, 859 (1973).

[35] T. Kawano, R. Capote, S. Hilaire, and P. Chau Huu-Tai, Phys. Rev. C **94**, 014612 (2016).

[36] E. S. Soukhovitskii, R. Capote, J. M. Quesada, and S. Chiba, Phys. Rev. C **72**, 024604 (2005).

[37] A. Gilbert and A. Cameron, Can. J. Phys. **43** (1965), 10.1139/p65-139.

[38] T. Kawano, S. Chiba, and H. Koura, Journal of Nuclear Science and Technology **43**, 1 (2006).

[39] R. Capote, M. Herman, P. Obložinský, P. G. Young,

S. Goriely, T. Belgya, A. V. Ignatyuk, A. J. Koning, S. Hilaire, V. A. Plujko, M. Avrigeanu, O. Bersillon, M. B. Chadwick, T. Fukahori, Z. Ge, Y. Han, S. Kailas, J. Kopecky, V. M. Maslov, G. Reffo, M. Sin, E. S. Soukhovitskii, and P. Talou, Nuclear Data Sheets **110**, 3107 (2009).

[40] J. Kopecky and M. Uhl, Phys. Rev. C **41**, 1941 (1990).

[41] M. Herman, R. Capote, M. Sin, A. Trkov, B. V. Carlson, P. Obložinský, C. M. Mattoon, H. Wienke, S. Hoblit, Y.-S. Cho, G. Nobre, V. Plujko, and V. Zerkin, *EMPIRE-3.2 Malta, Modular system for nuclear reaction calculations and nuclear data evaluation User's Manual*, Tech. Rep. INDC(NDS)-0603 (International Atomic Energy Agency, 2013).

[42] J. L. Ullmann, T. Kawano, T. A. Bredeweg, A. Couture, R. C. Haight, M. Jandel, J. M. O'Donnell, R. S. Rundberg, D. J. Vieira, J. B. Wilhelmy, J. A. Becker, A. Chyzh, C. Y. Wu, B. Baramsai, G. E. Mitchell, and M. Krtička, Phys. Rev. C **89**, 034603 (2014).

[43] K. Shibata, O. Iwamoto, T. Nakagawa, N. Iwamoto, A. Ichihara, S. Kunieda, S. Chiba, K. Furutaka, N. Otuka, T. Ohsawa, T. Murata, H. Matsunobu, A. Zukeran, S. Kamada, and J. Katakura, J. Nucl. Sci. Technol. **48**, 1 (2011).